ARTICLE

Correlations Between the Biochemistry and Mechanical States of a Sea-Urchin Ligament: A Mutable Collagenous Structure

A. R. Ribeiro · A. Barbaglio · M. J. Oliveira · R. Santos · A. V. Coelho ·
C. C. Ribeiro · I. C. Wilkie · M. D. Candia Carnevali · M. A. Barbosa

Abstract Mutable collagenous tissues (MCTs) of echinoderms can be regarded as intelligent and dynamic biomaterials, due to their ability to reversibly change their mechanical properties in a short physiological time span. This mutability phenomenon is nervously mediated and involves secreted factors of the specialized 'juxtaligamental' cells, which, when released into the extracellular matrix (ECM), change the cohesive forces between collagen fibrils. MCTs exist in nature in several forms, including some associated with echinoderm autotomy mechanisms. Since the molecular mechanism of mutability is still incompletely understood, the aim of this work was to provide a detailed biochemical analysis of a typical mutable collagenous structure and to identify possible correlations between its biochemistry and mechanical states. A better understanding of the mutability phenomena is likely to provide a unique opportunity to develop new concepts that can be applied in the design of dynamic biomaterial for tissue regeneration, leading to new strategies in regenerative medicine. The MCT model used was the compass depressor ligament (CDL) of a sea urchin (*Paracentrotus lividus*), which was analyzed in different mechanical states, mimicking the mutability phenomenon. Spectroscopic techniques, namely Fourier transform infrared (FT-IR) and confocal Raman microscopy, were used to identify the specific molecular components that contribute to the CDL biochemical microenvironment and to investigate the possibility that remodelling/synthesis of new ECM components occurs during the mutability phenomenon by analogy with events during pregnancy in the uterine cervix of mammals (which also consists mainly of mechanically adaptable connective tissues). The results demonstrate that CDL ECM includes collagen with biochemical similarities to mammalian type I

A. R. Ribeiro · M. J. Oliveira · C. C. Ribeiro ·
M. A. Barbosa (✉)
INEB-Instituto de Engenharia Biomédica, Universidade do
Porto, Rua do Campo Alegre 823, 4150-180 Porto, Portugal
e-mail: mbarbosa@ineb.up.pt

A. R. Ribeiro
FEUP-Faculdade de Engenharia da Universidade do Porto,
Rua Dr. Roberto Frias, 4200-645 Porto, Portugal

A. Barbaglio · M. D. C. Carnevali
UNIMI-Department of Biology, University of Milano,
Via Celoria 26, 20133 Milan, Italy

M. J. Oliveira
FMUP-Faculdade de Medicina da Universidade do Porto,
Alameda Prof. Hernâni Monteiro, 4200-319 Porto, Portugal

R. Santos · A. V. Coelho
Instituto de Tecnologia Química e Biológica, Universidade
Nova de Lisboa, Apartado 127, 2780-901 Oeiras, Portugal

R. Santos
Unidade de Investigação em Ciências Orais e Biomédicas,
Faculdade de Medicina Dentária, Universidade de Lisboa,
Cidade Universitária, 1649-003 Lisbon, Portugal

C. C. Ribeiro
ISEP-Instituto Superior de Engenharia do Porto,
Dep. de Física, Rua Dr. António Bernardino
de Almeida 431, 4200-072 Porto, Portugal

I. C. Wilkie
Department of Biological and Biomedical Sciences,
Glasgow Caledonian University, 70 Cowcaddens Road,
Glasgow G4 0BA, Scotland, UK

M. A. Barbosa
ICBAS-Instituto de Ciências Biomédicas Abel Salazar,
Universidade do Porto, Porto, Portugal

collagen, as well as sulphated glycosaminoglycans (GAGs). CDL mutability seems to involve a molecular rearrangement of the ECM, without synthesis of new ECM components. Although there were no significant biochemical differences between CDLs in the various mechanical states were observed. However, subtle adjustments in tissue hydration seemed to occur, particularly during stiffening.

1 Introduction

Mutable collagenous tissues (MCTs) are unusual morpho-functional adaptations of echinoderms [1–3]. They are considered to be "smart", or "intelligent", connective tissues due to their ability to reversibly change their biomechanical properties in a short time-scale, under nervous control [1–4].

Recently published data from our group [5] confirm that the compass depressor ligament (CDL) of the sea-urchin masticatory apparatus (Aristotle's lantern) has a typical MCT structure, consisting of a dense parallel array of collagen fibrils, which are surrounded by glycosaminoglycans (GAGs), proteoglycans (PGs) and a network of fibrillin-containing microfibrils, as well as specialized cells called juxtaligamental cells (JLCs) [4, 5].

The fibrils that dominate the CDL extracellular matrix (ECM) consist of collagen, the most abundant structural protein in the connective tissues of both invertebrates and vertebrates [6–8]. During the last decade, numerous investigations have characterized the fibrillar collagen chains in cnidarians, annelids, and sea-urchins, supporting the concept that in invertebrates and vertebrates the triple helix is conserved [9], despite the presence of some imperfections and sometimes low levels of sequence identity [6–8]. Several types of fibrillar collagen can be found in ECMs. The most abundant in echinoderms is type I, which is constituted by two $\alpha1$ (I) chains and one $\alpha2$ (I) chain, that were previously identified in echinoderms, namely in sea-urchin embryos and adult tissues of *Paracentrotus lividus* [9–14].

Regarding phylogenetic relationships, available data on the morphology and molecular biology of collagens from different MCTs indicate that they are evolutionarily close to vertebrate fibrillar collagens (type I) in terms of their structure, chain composition and gene organization [2–4, 9–16]. MCTs collagen fibrils are spindle-shaped with paraboloidal tips, a perfect shape for fibrils to reinforce the ECM. The Fibrils resemble those of mammalian connective tissues in composition and structure: they have a triple helix that assembles in parallel arrays with a regular stagger of 67 nm (similar to the banding pattern of mammalian type I collagen), have analogous cross-striations (with some differences in amino acids constitution) and are

stabilised by hydroxypyridinium intermolecular crosslinks [2, 10, 15, 16].

It has been suggested that the reversible modulation which underpins the mutability phenomenon does not result from effects on the structure and mechanical properties of collagen fibrils, but from the physiological control of interfibrillar cohesion [2, 3]. One potential stiffening molecule involved in the interfibrillar cohesion is tensilin, a protein present in the dermis of holothurians (sea-cucumbers) that was first characterized and purified by Tipper et al. [17]. It has been proposed that this molecule forms interfibrillar bridges between collagen fibrils, preventing interfibrillar slippage and increasing the resistance of the tissue to tensile forces [2, 3, 17, 18].

Concerning the mechanism of mutability, it is known that the CDL exhibits different mechanical states, which we have called "standard", "compliant" and "stiff" [5]. In this paper correlations between extracellular and cellular constituents of the CDL and the various mechanical states have been established. For instance, the mean interfibrillar distance of stiff CDLs was significantly lower than that of standard or compliant CDLs. The denser fibril packing of the stiff state is probably a result of the stretching of the CDLs in acetylcholine-stimulated preparations. It has been hypothesized that such shortening of the distance between adjacent fibrils would favour stiffening [5]. Concerning the cellular elements present in CDLs, juxtaligamental cells (JLCs) containing granules of varying electron density, were identified in the same investigation. There appeared to be a correlation between the darker granules of maturation, and the different mechanical conditions. A significant decrease in the number of 'dark' granules when CDLs shift from standard to compliant and from standard to stiff mechanical states, suggested that there are two populations of CDL granules, which could be functionally but not morphologically distinct [5]. The role of the intracellular granules of JLCs in mutability is probably crucial, since they store effector molecules such as tensilin that directly affect the interfibrillar cohesion of MCTs [2, 3, 5].

Proteoglycans (PGs) and glycosaminoglycans (GAGs) are also directly or indirectly involved in mutability, since they serve as binding sites for molecules responsible for interfibrillar cohesion. As reported for mammalian connective tissues, some interfibrillar PG bridges were visualized in CDLs, which were also preferentially located at specific sites in each D-period of the collagen fibrils [4, 5, 19–22].

GAGs were also identified through selective staining with alcian blue [5, 20]. Although non-covalently bound PGs identified biochemically in the spine ligament of another sea urchin [10] were shown to be sulphated, until now no attempts have been made to identify their presence in the CDL or their possible contribution to mutability.

Several studies reveal that MCTs are one of the key elements of echinoderm regenerative capacities [23, 24], since they provide a dynamic ECM with an optimal growth-promoting environment for tissue repair and regeneration. However, the mechanisms behind the capabilities of MCTs to assume distinct mechanical states are still enigmatic. Thus the main aim of this work was to contribute to the understanding of those mechanisms, bearing in mind their potential relevance for the development of implantable biomaterials for tissue regeneration. Existing biomaterials lack the inherent adaptability of natural tissues. In particular, they do not truly mimic the dynamic microenvironment of tissues and organs.

The present study was conducted because we believe that MCT is a source of inspiration for the development of a new class of biomaterials, with inherent dynamic properties. Spectroscopic techniques, such as FT-IR and confocal Raman microscopy, were used in order to reveal the biochemical fingerprint of the CDL. As there is a strong similarity between mammalian and MCT collagen, ultrapure collagen type I of bovine origin was used as control. Chondroitin sulphate from shark cartilage was used as a reference for GAG quantification, following a protocol described by Björnsson et al. [25]. Like chondroitin sulphates of various origins, shark cartilage contains chondroitin-4-sulfate and chondroitin-6-sulfate [26].

The possible correlation between CDL biochemistry and different mechanical states was investigated by spectroscopic techniques. Particular attention was given to adjustments in tissue hydration. The possibility of ECM remodelling (degradation and synthesis) occurring during mutability was also evaluated, since this is one of the mechanisms responsible for the mechanical adaptability of mammalian connective tissues, such as the uterine cervix during pregnancy [27–30].

2 Materials and Methods

2.1 Animal and Tissue Collection

In this study, the model used was the compass depressor ligaments (CDL) obtained from specimens of the sea-urchin *Paracentrotus lividus* collected on the north Portuguese coast, and maintained in an aquarium as described elsewhere [5]. The top half of the test ("shell") of an animal was removed and discarded in order to expose the masticatory apparatus, which contains ten CDLs. The half animal was then immersed in 0.1 % propylene phenoxetol (Sigma-Aldrich 484423) in seawater for 45 min, or in 1 mM acetylcholine (Sigma-Aldrich A6625) in seawater

for 15 min to obtain CDLs in the compliant and stiff states, respectively. Standard CDLs were obtained from half animals immersed in seawater. During all analyses, tissues were always kept in the specific solutions in order to maintain their respective mechanical states. All experiments were performed using five different animals.

2.2 Spectroscopic Characterization of CDL Microenvironment

2.2.1 Pure Components

Ultra-pure bovine collagen type I (Sigma-Aldrich C4243) and chondroitin sulphate sodium salt from shark cartilage (Sigma-Aldrich C4384) were used as reference for the identification of their corresponding components of the extracellular matrix of CDLs. Collagen films were prepared by mixing chilled (99 %) bovine collagen solution with 10x PBS. After pH adjustment to 7.2–7.6, 5 mL of collagen suspension were poured into a Petri dish ($\varnothing$ 35 mm) and kept at 37 °C for 1 h, in order to form a reticulated 3D gel. The gel was further dried in a vacuum system at room temperature to form a film. Chondroitin sulphate powder was analyzed as received.

2.2.2 Fourier Transform Infrared Spectroscopy (FT-IR)

Collagen films, chondroitin sulphate and hydrated CDLs in the different mechanical states were analyzed by FT-IR using a Perkin Elmer 2000 spectrometer. FT-IR analyses of CDLs were performed under wet conditions in the solutions described in Sect. 2.1, with exception of FT-IR analysis of CDL for protein conformation, which was carried out with dried tissues.

All the specimens were analyzed with attenuated total reflectance (ATR-FTIR) using the SplitPea™ accessory (Harrick Scientific), provided with a silicon internal reflection element and configured for external reflectance mode. Spectra were acquired from a 200 μm diameter sampling area. At least five different areas from each sample were analyzed. All samples were run at a spectral resolution of 4 cm^{-1} and two hundred scans were accumulated in order to obtain a high signal-to-noise ratio. A nitrogen purge of the sample compartment was performed to minimize artifacts that could arise from residual air bands (CO_2 and H_2O vapour). All spectra were automatically smoothed, and normalized using Spectrum software, version 5.3. The heights of the peaks of amide I (1,640 cm^{-1}, C=O stretch), amide II (1,550 cm^{-1}, C–N stretch and N–H in-plane bend), 1,450 cm^{-1} (CH bending) and the one between 3,100 cm^{1} and 3,600 cm^{-1} (OH and NH) of CDLs and collagen spectra were measured using the software Spectrum version 5.3.

2.2.2.1 Spectral Curve Fitting In order to identify the secondary structure of collagen (the main protein present in CDL ECM), ultrapure collagen films (reference) and CDLs were analyzed by FT-IR spectroscopy using the Mercury-Cadmium-Telluride (MCT) detector. Samples were maintained at room temperature in a vacuum system for 24 h to evaporate water. Spectral acquisitions were obtained as described before (Sect. 2.2.2).

Derivative and curve fitting algorithms were performed with the software PeakFit from AISN Software. One percent of smoothing was used in curve fitting method and initial peak positions were obtained from second derivative spectra of the raw data. The number and position of the peaks obtained were used as initial input parameters in the curve-fitting algorithm. A Lorentzian band-shape was used to fit the contours [31, 32]. The curve-fitting algorithm creates Lorentzian bands that are added to produce a computed spectrum, which is compared with the experimental one. The process is iterated until a satisfactory fit between the computed and experimental bands is obtained by a least square regression analysis. The calculated area of each sub-band is reported as a percentage of the computed contour. Once the adequate curve fitting was achieved for type I ultra-pure collagen, every parameter was then fixed for the analysis of CDL spectra [31, 32]. To obtain correct band area determinations, curve fitting was performed on larger spectral intervals than those used for peak assignment to avoid anomalous band addition during curve fitting that could result in significant errors. Protein secondary structure parameters were further assessed using absorption bands assigned as α-helix, triple helix, β-sheets, β-turns, and unordered structure (% of total amide I absorption). The curve fitting procedure was applied to 1,480–1,720 cm^{-1} [ν(C=O) amide I absorption] interval which allows the determination of collagen secondary structure parameters. Furthermore, other spectral regions giving additional information and contributing to the classification of collagen types, namely the intervals 1,350–1,480 cm^{-1} [δ(CH$_2$) and δ(CH$_3$) absorptions], 1,180–1,300 cm^{-1} [ν(C–N) and δ(N–H) of amide III] and 1,005–1,100 cm^{-1} [ν(C–O) and ν(C–O–C) absorptions of carbohydrate moieties], were also investigated.

2.2.3 Confocal Raman Spectroscopy

A LabRAM HR 800 confocal Raman microscope system (Horiba-JobinYvon) comprising a spectrometer and a fully integrated confocal microscope Olympus BX41 was used to characterize hydrated CDLs in the different mechanical states, as well as collagen films and chondroitin sulphate powder. All analyses were conducted on samples placed on CaF$_2$ discs. Raman spectra were generated using 785 nm laser diode as excitation source with an effective laser power of 6 mW, focused on the sample with a 100x or a 50x (LWD) objective for analysis in liquids. The scattered light was dispersed by a grating with 1,800-lines/mm (Jobin–Yvon), and a thermoelectrically cooled charged-coupled detector (CCD) camera recorded the spectra. The CCD was connected to a computer for data collection and analysis using Labspec software (Horiba JobinYvon, Lille, France), OriginPro data analysis and graphing software. Collagen and chondroitin sulphate spectral acquisitions were performed in 400–1,800 cm^{-1} wavenumber range using the following conditions: exposure time 100 s, five accumulations, confocal pinhole 100 μm, spectral resolution 4 cm^{-1}. In order to avoid CDL tissue dehydration, Raman analyses were performed with a Long Working Distance (LWD) objective in the conditioning media (propylene phenoxetol, acetylcholine and seawater) that mimic the in vivo states. Previous to the analysis, several experimental parameters were optimized namely volume of solution, exposure time and power of the incident laser, in order to avoid any possible dehydration/degradation of the tissues during spectral acquisition. All CDLs were analyzed immersed in 20 μl of solution. The liquid environment also offers the advantage of dissipating the heat generated by the laser beam, thus preventing tissue damage. Spectral data were acquired in different areas of the sample. All spectra were baseline corrected and smoothed, using an automatic polynomial function and vector normalized on the whole spectra. Additional data manipulation included standard signal averaging and cosmic event (spike) removal.

2.2.3.1 Ex Vivo Determination of Water Concentration Profiles in CDL in the Different Mechanical States The water content of tissues was determined from the ratio of Raman intensities of the OH stretch vibration of water at 3,390 cm^{-1} and the CH$_3$ stretch of protein at 2,935 cm^{-1}. Hydration measurements were carried out on CDLs in the different mechanical states and in five different animals. Samples were analyzed using a 785 nm laser as the excitation source. Water concentration profiles were obtained by acquiring Raman spectra at different depths below CDL surface at 20 μm increments. For determination of water/protein ratios in CDL we used the ratio of the integrated intensities of water (3,350–3,550 cm^{-1}) and protein (2,910–2,965 cm^{-1}) in order to maximize the signal-to-noise ratio and avoid overlap of the water signal with the NH vibration of protein at 3,329 cm^{-1}. The signal collection time per spectrum was 5 s.

2.3 Tissue Hydration Assay

Tissue hydration of CDLs in different mechanical states was evaluated by subtracting the dry from the wet weight

and dividing by the wet weight. Dry weight was measured after a thermal treatment performed in a Perkin Elmer Differential Scanning Calorimeter (DSC), where tissues were heated from 5 to 180 °C, for 60 min, in order to ensure complete dehydration.

2.4 Sulphated Glycosaminoglycan Quantification with Alcian Blue

The concentration of sulphated GAGs in CDLs in the different mechanical states was measured according to the procedure of Björnsson et al. [25]. This protocol uses alcian blue, a cationic dye that is able to bind to sulphated GAGs. GAGs were extracted from CDLs in different functional states after immersion in 4 M guanidine-HCl for 15 min, at 4 °C. GAGs were then precipitated with alcian blue 8GX dye (Sigma-Aldrich A9186-10G) stock solution (alcian blue in 0.1 % H_2SO_4/0.4 M guanidine-HCl) after overnight incubation at 4 °C, and collected by centrifugation (15 min, 12,000g). The excess stain and contaminating proteins were removed by washing the pellet in DMSO-$MgCl_2$ for 15 min. The proteoglycan-alcian blue complexes were then immersed in guanidine-HCl/propanol until completely dissolved. After dissociation of the complex, the GAG concentration was determined spectrophotometrically ($\lambda = 605$ nm) using the corresponding calibration curve established with chondroitin sulfate sodium salt from shark cartilage (Sigma-Aldrich C4384) as the standard, since the amount of GAG/PGs is directly proportional to the alcian blue concentration. The sulphated GAG concentration was normalized with reference to wet tissue weight.

2.5 Protein Extraction and Identification

2.5.1 Protein Extraction and Separation by 1D SDS-PAGE

Animals were immersed in specific solutions (see Sect. 2.1) in order to obtain CDLs in the standard, stiff and compliant states. After immersion, tissues were cut in RIPA lysis buffer (200 mM Tris–HCl buffer pH 7.5 plus 1 % Triton-X 100, 150 mM NaCl and 1 % of NP-40), homogenized, and sonicated during 30 min at 4 °C to allow the solubilization of proteins. Protein concentration was determined using a DC Protein Assay kit from Bio-Rad (500-0112). For gel electrophoresis, 25 µl of sample buffer (1610791 XT sample buffer from Bio-Rad) in 5 µl of reducing agent (161-0792 XT Reducing Agent from Bio-Rad) were added to the 25 µg of CDLs extracts and the resulting solution was heated for 5 min at 95 °C. Protein separation was achieved using Criterion™ XT Tris–Acetate Gel, 3–8 % from Bio-Rad (345-0129-MSDS), and electrophoresis was carried out at a constant voltage of 150 V. Ten µl of protein standard (HiMark™ Pre-stained Protein Standard, ref. LC 5699 from Invitrogen) was used for molecular weight (MW) determination. The separated proteins were visualized by staining overnight with very sensitive Colloidal Coomassie Brilliant BlueG 250 (Sigma 27816).

2.5.2 Protein Identification by Mass Spectrometry: In-Gel Digestion

Protein bands were removed from the gels using a disposable scalpel and were digested as previously described [33, 34]. Milli-Q H_2O was used to wash the excised bands that were subsequently destained in 50 % (V/V) and 100 % acetonitrile (ACN). Disulfide bonds were reduced with 10 mM DTT and alkylated with 50 mM iodoacetamide, the excised bands were allowed to swell in a digestion buffer (50 mM NH_4HCO_3) containing 6.7 ng/µL of trypsin (modified porcine trypsin, sequencing grade; Promega, Madison, WI, USA) on an ice bath. The supernatant was removed after 30 min, and 20 µL of 50 mM NH_4HCO_3 was added to the gel pieces for digestion, which was performed overnight at 37 °C. After complete digestion, the supernatant was stored at −20 °C until used [33, 34].

2.5.3 MALDI–MS/MS

The digested peptides were desalted and concentrated using home-made chromatographic microcolumns packed with different affinity materials, as described elsewhere [33–35]. Briefly, constricted GELoader tips (Eppendorf) were packed with POROS R2 chromatographic resin (PerSeptiveBiosystems) or graphite powder (activated charcoal; Sigma-Aldrich) [33–35]. Then, each digested spot was subsequently passed through R2 and graphite microcolumns and eluted separately onto the MALDI plate using 0.5 µl of 5 mg/mL CHCA in 50 % (v/v) ACN with 2.5 % (v/v) formic acid.

Mass spectrometry was performed using a MALDI–TOF/TOF 4800 plus mass spectrometer (Applied Biosystems). The mass spectrometer was externally calibrated using des-Arg-Bradykinin (904.468 Da), angiotensin 1 (1,296.685 Da), Glu-Fibrinopeptide B (1,570.677 Da), ACTH (1–17) (2,093.087 Da), and ACTH (18–39) (2,465.199) (4700 Calibration Mix, Applied Biosystems). Each reflector MS spectrum was collected in a result-independent acquisition mode, typically using 1,000 laser shots per spectra and a fixed laser intensity of 3,500 V. The fifteen strongest precursors were selected for MS/MS, the weakest precursors being fragmented first. MS/MS analyses were performed using CID (Collision Induced Dissociation) assisted with air, with collision energy of 1 kV and gas pressure of 1×106 torr. Two thousand laser shots were collected for each MS/MS spectrum using a fixed

laser intensity of 4,500 V. Raw data were generated by the 4000 Series Explorer Software v3.0 RC1 (AB Sciex) and contaminant m/z peaks resulting from trypsin auto digestion were excluded when generating the peptide mass list used for database search. The interpretation of the combined MS and MS/MS data was carried out using the algorithm, MOWSE (provided with MASCOT; version 2.2; Matrix Science) and two different databases (UniProt/ Swiss-Prot joined together with the purple sea-urchin *Strongylocentrotus purpuratus* genome predicted protein database and UniRef100). The search was performed using monoisotopic peptide masses and the following criteria: one missed cleavage, $p < 0.05$ significance threshold, 50 ppm peptide mass tolerance, 0.25 Da fragment mass tolerance, carbamidomethylation of cysteine as fixed modification, and methionine oxidation as variable modification. Spectra with significant hits were visually inspected to eliminate false positives [33, 34, 36].

2.6 Statistical Analysis

At least five experiments were performed for each analysis. Statistical differences between CDLs in different functional states were determined using Kruskal–Wallis one-way analysis of variance (ANOVA) with Dunn's post hoc test. Data are given as mean ± standard deviation (SD). Results were considered statistically significant when $P < 0.05$. In Boxplot graph (Fig. 6b, c, d) the data represented are the minimum, lower quartile, median, upper quartile, and maximum.

3 Results

3.1 Biochemical Characterization of CDL Extracellular Matrix

3.1.1 Ex Vivo FT-IR Spectra of CDL

The extracellular matrix (ECM) of standard CDLs was analyzed by FT-IR (Figs. 1, 2) and Raman spectroscopy (Fig. 3) and compared with the spectra of mammalian collagen type I and shark chondroitin sulphate, used as positive controls.

A comprehensive assignment of the major bands was derived from the literature. The main bands of collagen (Fig. 1a) arose from the peptide bond vibrations: amide A (NH stretch), amide I (C=O stretch), II (C–N stretch and N–H in-plane bend) and III (C–N stretch, N–H bend and CO in-plane bend). The spectrum of chondroitin sulphate (Fig. 1b) exhibited features arising from COO^- (1,610 and 1,411 cm^{-1}) but also from sulphate (SO_4^{2-} at 1,240 cm^{-1}) and sugar (1,000–1,200 cm^{-1}) groups.

FT-IR spectra of CDL exhibited bands assignable to collagen, since the striking resemblance between the spectra was immediately apparent (Fig. 1a), confirming that collagen was the dominant protein present in CDL ECM, as previously implied by morphological data [1–5].

The characteristic absorbance bands of CDL were amide I (1,640 cm^{-1}), amide II (1,550 cm^{-1}) and amide III (1,239 cm^{-1}), arising from the peptide bond vibrations of the main structural proteins, namely collagen. The spectral region between 1,000 and 1,500 cm^{-1} was the most crowded in the CDL spectrum, due to the absorptions from many biologically important functional groups (such as CH_2, CH_3) bending vibration arising from lipids, as well as COO^- absorptions attributed to carbohydrate moieties, fatty acids and amino acid side chains.

As revealed in Fig. 1a, the major FT-IR bands of CDL and mammalian collagen overlapped markedly, making it difficult to identify GAGs and other components in the CDL spectrum. In order to overcome this limitation, the collagen spectrum was subtracted from that of the CDL. The resultant spectrum showed absorptions at 1,240–1,250 cm^{-1} (v (S=O)) and 825–850 cm^{-1} (v (C–O–S)) due to the presence of sulphates, apart from spectral features at 1,630–1,650 cm^{-1} and 1,552 cm^{-1} (amide I and II, respectively).

3.1.2 Determination of Protein Secondary Structure

FT-IR spectroscopy can provide information on the secondary structure content of proteins. Different collagen types exhibit similar IR absorption bands but can be distinguished by their secondary structures [31, 32]. The spectral region most sensitive to protein secondary structural components is the amide I band (1,700–1,600 cm^{-1}) which is due almost entirely to the stretch vibrations of the C=O peptide linkages. Figure 2 shows the deconvoluted spectra of collagen type I and CDL in the 1,550–1,700 cm^{-1} interval.

The decomposition of the collagen amide I band revealed several components (1,626, 1,647, 1,660, 1,670 and 1,690 cm^{-1}) that were observed in both collagen type I and CDL spectra. The curve fitting procedure applied to the amide I band of ultrapure collagen type I and CDL spectra allowed determination of secondary structure parameters of collagen according to the band positions: α-helix (1,660 cm^{-1}), β-sheets (1,679 and 1,626, 1,691 cm^{-1}), β-turns (1,608 and 1,669 cm^{-1}), triple helix (1,637 cm^{-1}) and random coil structure (1,647 cm^{-1}). Spectral area per band was used to calculate the percentage of secondary structures (Table 1) [31, 32].

It was found that deconvoluted spectra of collagen type I and CDL ligament show a predominance of triple helix and α-helix structures, compared to β-sheets. This could be
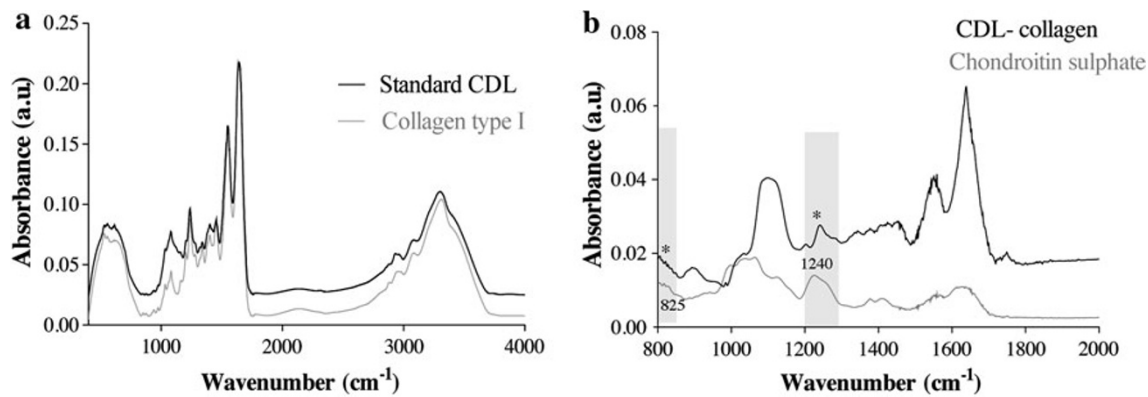
Fig. 1 Fourier transform infrared (FT-IR) spectra of: **a** standard CDL and bovine collagen type I. **b** The difference spectra of CDL and collagen type I (CDL-collagen) shown together with the spectrum of chondroitin sulphate from shark cartilage. The *grey areas* indicate characteristic wavenumber intervals for sulphate groups of chondroitin sulphate

Fig. 2 FT-IR deconvoluted spectra of Amide I absorption band: **a** ultrapure collagen type I; **b** standard CDL
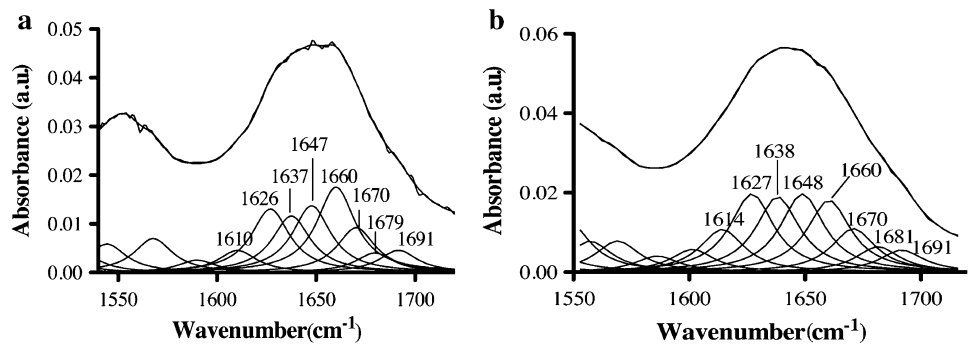
Fig. 3 Raman characterization of the CDL microenvironment: **a** video image of standard CDL (10× objective); **b** Raman spectra of collagen type I and standard CDL (*Asterisk* (*) indicates the presence of additional spectral features in CDL spectra); **c** difference between the spectra of CDL and collagen, together with the spectrum of chondroitin sulphate from shark cartilage (*Asterisk* (*) indicates the presence of sulphate groups of chondroitin sulphate)
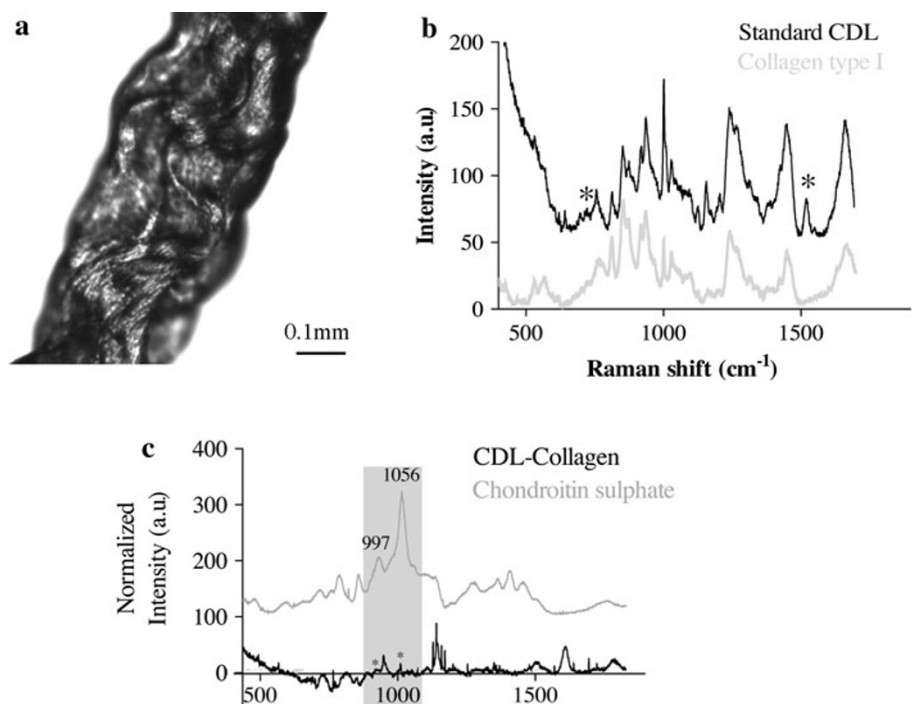
Table 1 Secondary structure (in %) of collagen type I from bovine origin and CDL (N = 5 for both collagen type I and CDL spectra)

	α-helix	β-sheets	β-turns	Triple helix	Unordered
Collagen type I	18 (±0.2)	31 (±1)	18 (±0.4)	17 (±1)	16 (±1)
CDL	15 (±2)	30 (±1)	19 (±0.8)	18 (±1.4)	18 (±2)

explained by the lack of globular domains in the protein. The presence of a triple helix structure on collagen type I and CDL was also confirmed by the mean absorption IR ratios between amide III at 1,239 cm^{-1} (CN stretch, NH bend and NH in-plane bend) and 1,454 cm^{-1} (CH bending) which were 1.19 (N = 5) and 1.18 (N = 5), respectively. Values higher than 1.0 indicated the presence of triple helices, in contrast to the 0.59 of gelatin (a protein devoid of a triple helix secondary structure) [37, 38].

Curve fitting of collagen films and CDL spectra (results not shown) in the intervals 1,350–1,480 cm^{-1} [$\delta(CH_2)$ and $\delta(CH_3)$ absorptions], 1,180–1,300 cm^{-1} [$v(C–N)$ and $\delta(N–H)$ amide III absorptions] and 1,005–1,100 cm^{-1} [$v(C–O)$ and $v(C–O-C)$ absorptions of carbohydrate moieties], presented differences in the number and position of the bands, suggesting that other collagen types could contribute to the CDL matrix, besides collagen type I. In the analysis of these data, it should be taken into consideration that intensity of spectral signal, as well as signal-to-noise ratio in those intervals, was significantly lower than in the amide I zone, a fact that could have influenced the quality of curve fitting.

3.1.3 Ex Vivo Raman Spectra of CDL

Raman measurements were performed on regions where the ECM was visibly abundant. Several predominant bands at 855, 939, 1,004, 1,245, 1,452 and 1,664 cm^{-1} were evident in Raman spectra of both collagen type I and CDL (Fig. 3). The peak in the 1,655–1,667 cm^{-1} region was assigned to the amide I band of collagen, the one at 1,452 cm^{-1} to the CH_2/CH_3 deformation of lipids and the one at 1,241–1,272 cm^{-1} to amide III. The presence of some amino acids, such as phenylalanine (1,003 cm^{-1}) and tyrosine (646 cm^{-1}), was also detected in both spectra.

Interestingly, the aromatic or saturated side chain rings of proline and hydroxyproline amino acids, present in the collagen structure, appeared in CDL spectra as two bands at 926 and 856 cm^{-1} for proline and 878 cm^{-1} for hydroxyproline. The peak at 939 cm^{-1} is related to C–C vibrations of the collagen backbone.

As with FT-IR, the Raman spectrum of CDL revealed the presence of sulphate groups of chondroitin-sulphate with main sulphate vibrations of OSO_3^- at 1,067 cm^{-1} and C–O–S vibration at 996 cm^{-1} (Fig. 3c).

Both in FT-IR and Raman spectra, CDL showed peaks with higher intensity than those of pure collagen type I, an observation that is correlated with the amount of organic contents absorbing radiation. In the CDL tissue, other components besides collagen, like nucleic acids, lipids and sugars, give rise to absorptions in the vibrational spectra, contributing to the increase in intensity in most spectral regions. Although there was a strong similarity between the collagen and CDL Raman spectra, additional spectral features were observed in the CDL spectrum (between 800–1,000 and 1,500–1,600 cm^{-1}), due to the presence of additional biochemical species in the ECM.

### 3.2 Biochemical Characterization of CDLs in the Different Mechanical States

3.2.1 Protein Identification and Sulphated Glycosaminoglycans Quantification

One-dimension gel electrophoresis showed a pattern of protein bands common to CDLs in the different mechanical states, with no significant differences being observed in terms of protein quantity. Numerous protein bands with apparent molecular masses ranging from 10 to 250 kDa were observed (Fig. 4). However, only the most intense were excised and identified using MALDI–TOF/TOF.

The combination of mass spectrometry with homology-database search, allowed the identification of the following proteins: actin, tubulin, myosin and major yolk. Bands 1 and 2 were identified as either muscle (41 kDa) or as cytoskeletal actins (42 kDa), respectively. Gel band 3 was identified as tubulin, and bands 4 and 7 as myosin bands. Gel bands 5 and 6 were identified as toposome protein (173 and 180 kDa) (Fig. 4a; Table 2). The remaining bands could not be identified despite the quality of the obtained MS and MS/MS spectra. Probably due to the heavy presence of post-translational modifications or to the lack of homology with protein sequences deposited in the searched database.

Concerning sulphated GAGs, no significant differences were found between CDLs in the various mechanical states. Any real differences may have been masked by the strong variability that was observed between animals and which was indicated by the large standard deviations (Fig. 4b). The high error bars are reminiscent of the inter-individual variability that has previously been reported in MCTs of *P. lividus* and other echinoderms [2–5].
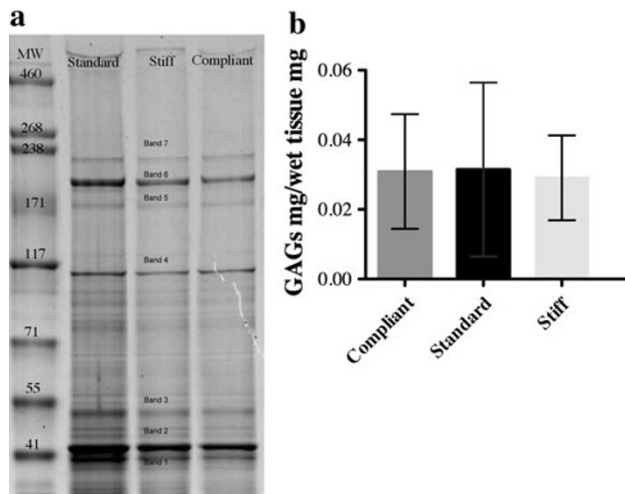
Fig. 4 Quantification of some ECM components of CDLs in the different mechanical states: **a** separation of proteins extracted from CDLs. Bands excised from in-gel digestion are numbered. **b** Sulphated GAG quantification with alcian blue staining (mean values). MW-molecular weight of marker proteins is shown in kDa at the *left*

3.3 Spectroscopy Characterization

FT-IR spectra obtained for CDLs in the different mechanical states were similar (Fig. 5). The mean IR ratios between amide III (1,239 cm^{-1}) and 1,454 cm^{-1} for CDL in the stiff and compliant condition were also higher than one: 1.8 (N = 5), 1.9 (N = 5) for stiff and compliant CDLs, respectively. The most noticeable difference concerned the amide I/amide II intensity ratio. Stiff CDLs presented a significantly higher amide I/amide II intensity ratio than did compliant tissues. The characteristic bands in the infrared spectra of proteins that include the amide I and amide II arise from peptide bonds. Absorption associated with the amide I band leads to stretching vibrations of the C=O bond of the amide, whereas absorption associated with the amide II band leads primarily to bending vibrations of the N–H bond.

Non-protein components of tissues also contributed significantly to the amide I region of the spectrum, the most intense arising from the O–H vibration of water (a band around 1,640 cm^{-1}). Consequently, the variation of the amide I/amide II intensity ratio can be related to both the protein and water content of the tissues. The collagen type I film also showed a lower amide I/amide II intensity ratio, compared with CDLs.

3.4 Contribution of Water to CDL Mutability Phenomena

The broad band in the 3,100–3,600 cm^{-1} region of the FT-IR spectra (Fig. 5a) results from the overlapping of the absorption bands of O–H groups from water molecules, N–H groups from proteins, and NH$_2$ groups from nucleic acids. The quantitative estimation of the mean band intensity in this frequency region, which is provided in Fig. 5c, suggests a higher water content in stiff tissues compared with the compliant and control ones. However, no statistically significant differences were observed between the amounts of water present in the three mechanical states of CDLs when water loss was estimated by heating (Fig. 6a). In order to elucidate this aspect, we decided to investigate if the amount of water varied from the periphery to the centre of the tissues. For that, Raman spectra were collected at different depths. Data indicate that in stiff tissues there is a decrease in water content from the surface to the bulk tissue (Fig. 6d), probably as a result of water exudation, whereas in the compliant and standard condition (Fig. 6b and c), the bulk is more hydrated.

4 Discussion

4.1 CDL Biochemical Microenvironment

As in mammalian connective tissues, the ECM of the CDL consists mainly of collagen fibrils with a structure (D-banding periodicity 59.2 ± 6.2 nm), chain composition and gene organization similar to that of vertebrate type I collagen [2–5, 9–16]. About 30 collagen types have been already identified. However, sea urchin collagen has been found to have two α1 (I) chains and one α2 (I) chain, which is characteristic of collagen type I [9, 12–14]. Taking this into consideration we used high purity bovine collagen type I as a positive control in our investigation. CDL and commercial collagen type I were analyzed by infrared and confocal Raman spectroscopy, in order to obtain detailed information on molecular structure, composition and microenvironment of CDLs. In the present study, we combined information obtained with both techniques, in order to obtain maximum information concerning differences/similarities between CDL and bovine collagen. Even though both spectroscopic techniques probe molecular vibrations and structure, they do not provide exactly the same information, and are complementary in nature.

FT-IR and Raman data revealed that collagen made a strong contribution to the CDL spectrum, and demonstrated the presence of amino acid side chains characteristic of collagen, such as proline and hydroxyproline, as well as other constituents like carbohydrates, fatty acids, nucleic acids and phospholipids [2–5, 39–47].

Infrared spectroscopy is a well-established experimental technique for the analysis of secondary structure of protein, which has been used to differentiate between collagen types on the basis of structural parameters [31, 32, 48–52].

Table 2 Proteins identified in ECM of CLD from the sea-urchin *Paracentrotus lividus* identified by MALDI–TOF/TOF–MS of in-gel tryptic digests of the bands indicated in Fig. 4a

Gel band	Protein name	Species	Accession number[a]	Database	Protein score[b]	Peptide score[b]	Number of distinct peptides[c]
1	Predicted similar to cytoskeletal actin	*Strongylocentrotus purpuratus*	gi|72007954	Uniprot-SwissProt/S.p.	791	662	16
2	Predicted similar to cytoskeletal actin	*Strongylocentrotus purpuratus*	gi|72007954	Uniprot-SwissProt/S.p.	749	631	15
3	Tubulin alpha-1 chain	*Paracentrotus lividus*	P18258	Uniprot-SwissProt/S.p.	569	496	11
4	Predicted similar to myosin heavy chain	*Strongylocentrotus purpuratus*	gi|115692122	Uniprot-SwissProt/S.p.	661	580	23
5	Predicted similar to major yolk protein precursor	*Strongylocentrotus purpuratus*	gi|115924727	Uniprot-SwissProt/S.p.	137	118	8
	Toposome	*Paracentrotus lividus*	Q6WQT5	UniRef100	265	151	17
6	Major yolk protein	*Strongylocentrotus purpuratus*	gi|47551123	Uniprot-SwissProt/S.p.	226	212	9
	Toposome	*Paracentrotus lividus*	Q6WQT5	UniRef100	873	673	32
7	Predicted similar to myosin heavy chain	*Strongylocentrotus purpuratus*	gi|115692122	Uniprot-SwissProt/S.p	900	766	31

Peptide mass (MS) and fragmentation (MS/MS) data were used to search against the UniProt/Swiss-Prot database joined together with the purple sea urchin *Strongylocentrotus purpuratus* genome predicted protein database and UniRef100. A confident index of 100 % was obtained in all cases

[a] Accession numbers of the identified protein in UniProt-SwissProt/S.p. or Uniref100 databases

[b] *Mowse* scoring algorithm corresponding to a confidence index for which the protein/peptide match was not random

[c] Peptide whose sequence differs in at least 1 amino acid residue

The amide group vibrations of protein backbones received particular attention, since they are present in all proteins and provide information on protein secondary conformation [47, 50, 51]. The most sensitive spectral region to the protein secondary structural components is the amide I band (1,700–1,600 cm^{-1}). High sensitivity to small variations in molecular geometry and hydrogen bonding patterns makes the amide I band uniquely useful for the analysis of protein secondary structural composition and conformational changes [51, 52]. However, the observed amide I bands of proteins are usually of little practical interest, due to the extensive overlap of the broad underlying component bands that lie in close proximity to one another, rendering instrumental resolution practically impossible [51]. As a consequence, mathematical methods are necessary to resolve the individual band component corresponding to specific secondary structure. Derivative and curve fitting methods can be applied to quantify the area of each component ascribable to a particular secondary structure (α-helix, β-sheet, random and turn structures).

Using an approach similar to that of Petibois et al. [32], curve fitting was performed for different regions of the FT-IR spectra of collagen and CDLs, and particular attention was given to the amide I zone, since its shape is sensitive to the type and amount of secondary structures and is not influenced by side chains [31, 32, 48]. Studies described in the literature showed that it is possible to distinguish several types of collagen (dried samples) based on its secondary structure [31, 32, 48]. In particular, type I collagen can be distinguished from type IV by higher amounts of triple helix and α-helix but lower amounts of β-sheets. In our study, we have compared a commercially available type I collagen with collagen from CDLs. The results confirmed that CDL collagen has a triple helical structure and has strong similarities to mammalian type I collagen. However, differences were observed in other spectral regions, suggesting the presence of other types of collagen. This is expected, since mature connective tissues of mammals, such as cornea, skin, and cartilage, contain heterotypic collagen fibrils consisting of more than one collagen type [6, 53].
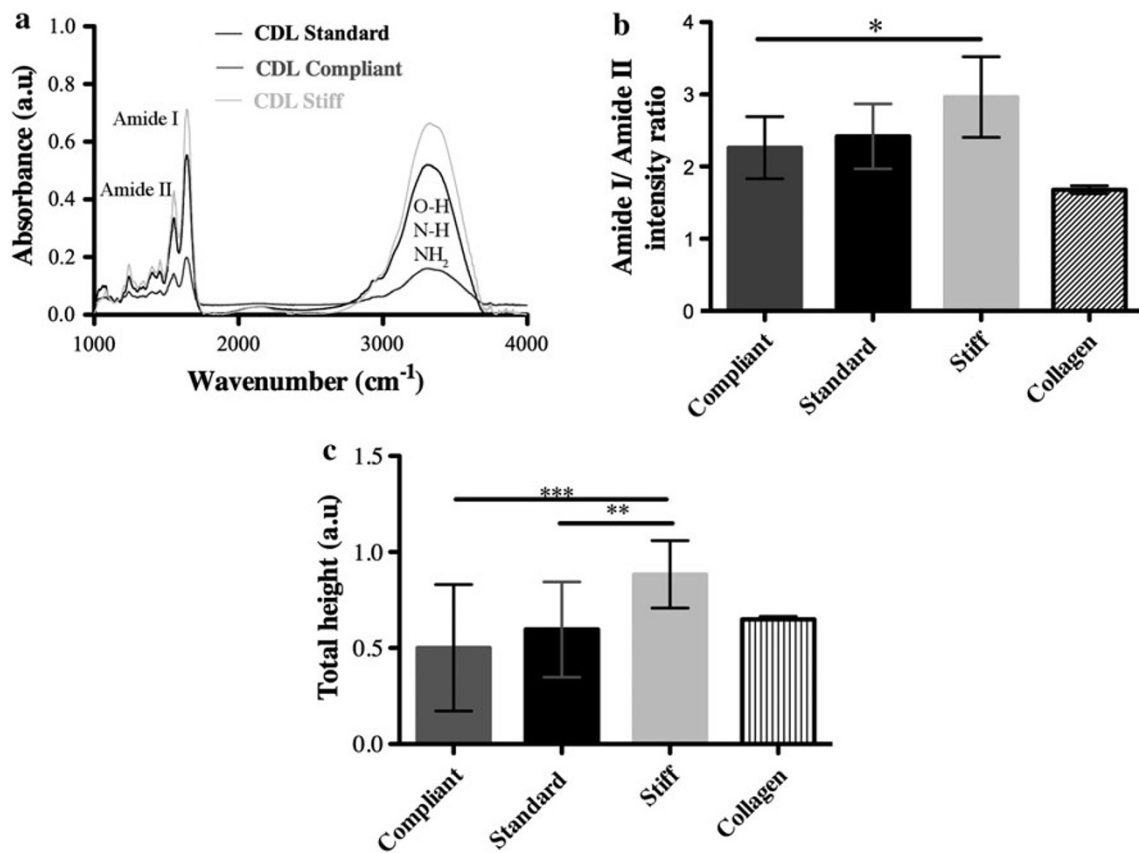
Fig. 5 FT-IR characterization of CDLs in the different mechanical conditions: **a** FT-IR spectra of CDL and **b** mean amide I/amide II intensity ratio for CDL in the compliant, standard, and stiff mechanical conditions, as well as for collagen (N = 15).

c Quantitative estimation of the mean intensity band in the frequency region $3,100$–$3,600$ cm^{-1} present in FTIR spectra. *Asterisk* (*) represents statistically significant differences *P < 0.05; **P < 0.01; ***P < 0.001

Mutable collagenous tissues can be considered as composite materials, comprising not only a dense extracellular matrix of collagen fibrils but also fibrillin microfibrils, PGs, specific effector molecules (constitutive and regulative proteins), and also water [1–5]. As in mammalian connective tissues, some of the molecules involved in interfibrillar cohesion are PGs that are covalently or noncovalently attached to collagen fibrils, serving as binding sites for the effector molecules responsible for interfibrillar cohesion (e.g. tensilin) [2, 17, 18].

In addition to collagen, PGs were previously identified in the CDL by histochemical methods [5]. It was shown that they are located at specific and periodic sites on the collagen fibril surface and their GAG side-chains were labelled by alcian blue [5]. The spectroscopic characterization performed in the present investigation identified sulphate spectral features (chondroitin sulphate) in CDLs [54–60]; nevertheless, the possible existence of non-sulphated GAGs cannot be excluded. Sulphated GAGs have been identified in other mutable collagenous structures of echinoderms [10, 20, 22]. Sulphated GAGs appear to have been conserved in invertebrate evolution, possibly because, in addition to their structural role in

connective tissues, they contribute to protective reactions against foreign bodies [61, 62].

4.2 Remodelling or Reorganization of CDL During Mutability Phenomena?

Dynamic ECMs are not exclusive to echinoderms; mammals also have mechanically adaptable connective tissue in the uterine cervix, which is normally rigid, but becomes very pliant during pregnancy, thereby allowing delivery [27–30, 63–66]. This mutable connective tissue passes through different stages (ripening, dilatation and post-partum) that are coordinated by neuro-endocrine mechanisms, but differs from echinoderm MCTs in the much longer time course (hours to days) of the tensile changes. In this case, the reversible changes in mechanical properties result from modifications of the biochemical composition and structure of the cervix, where matrix metalloproteinases have an important role in ECM degradation. So far, no relationship between collagen (type I and III) content and the variations in the tensile strength have been detected or established. The increase in tissue compliance is strongly correlated

Fig. 6 Role of water in mutability: **a** weight loss of CDL after thermal treatment. Water content at depth increments calculated from the intensity ratio of OH band ($3,350 \ cm^{-1}$) and protein bands ($2,910$–$2,965 \ cm^{-1}$) for **b** compliant, **c** standard and **d** stiff CDLs (Raman results)
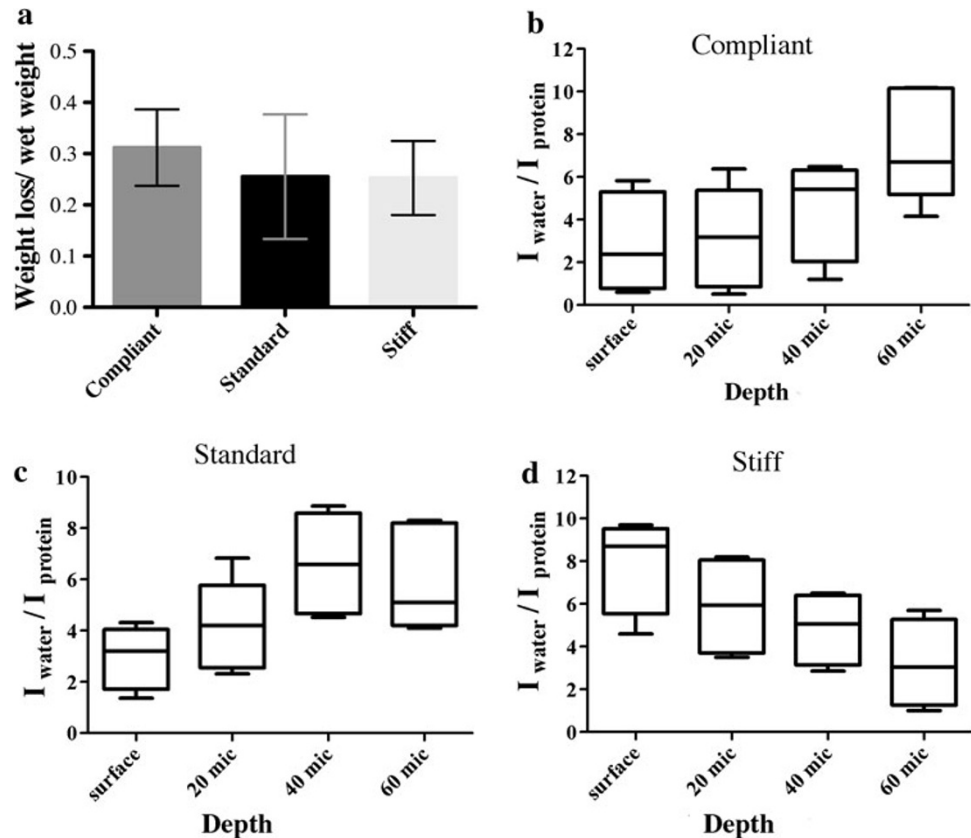
with the synthesis of collagen with higher solubility and fewer cross-links, and also with changes in biochemical composition, collagen degradation, increase in tissue GAG content and tissue hydration [27–30, 63–66]. Finally, after labour there is a significant increase in the transcription of genes involved in matrix repair, leading to ECM remodelling and recovery of tissue integrity [27–30, 63–66].

A novel objective of the present study was to look for evidence of ECM remodelling during mutability, One-dimension gel electrophoresis tests indicated that other proteins besides collagen are present in CDLs. However, protein pattern and quantity are the same in ligaments in different mechanical states. FT-IR data suggest that subtle adjustments of protein content may occur in stiff CDLs. However, it is possible that these are due to the release of protein effectors, such as tensilin into the ECM.

No significant differences in the content of sulphated GAGs in CDLs in different mechanical states was observed, suggesting that sulphated GAGs act exclusively as binding sites for effector molecules (e.g. tensilin). Further work needs to be done to look for non-sulphated GAGs in the CDL.

An important difference between cervical tissue and CDL destiffening is that the former seems to occur partly through the degradation of collagen fibrils [27–30, 63–66], whereas there is no evidence that this accompanies the destiffening of echinoderm MCTs [2, 3, 5]. No

morphological degradation of collagen fibrils was associated with the variable tensility of CDLs, as suggested by Ribeiro et al. [5], implying that CDL mutability is the result of molecular rearrangement. The IR ratios of Amide III and the peak positioned at $1,450 \ cm^{-1}$ of CDLs in the different mechanical conditions were higher than 1.0, demonstrating that variable tensility of CDLs does not involve changes in the molecular conformation of collagen molecules [31, 32, 67–69]. Given that collagen is a very stable protein, and mutability occurs in short physiological time-scales, it is highly unlikely that there is enough time for stiffening to result from the synthesis of new collagen.

A first trial to identify the proteins involved in CDL mutability by mass spectrometry conjugated with protein database search using the recently sequenced genome and predicted protein database of purple sea urchin, *S. purpuratus* [36] was also performed. Amongst the identified proteins are two structural proteins, tubulin and actin, whose presence is related to the cellular elements of the CDL. Myosin was also identified, which was expected since a myoepithelium occupies around 8 % of the CDL cross-sectional area [4]. Although bands 5 and 6 could represent major yolk protein, a very abundant glycoprotein of the coelomic fluid that surrounds the CDL, a higher score was observed with toposome from *P. lividus* [70]. Toposome is a protein essential for sea-urchin cell

adhesion and development [71]. Further work on protein extraction protocols, as well as other separation techniques, is being carried out, in order to identify possible key-proteins involved in CDL mutability.

4.3 The Contribution of Water to the Mutability Phenomena

The ECM of CDLs is complex, like most ECMof stiff CDLs increases from surface to bulk, suggestings. The matrix is comparable to a hydrogel due to the high water content (80–90 % in sea-cucumber dermis), where GAGs that link fibrillar structures have an important role in maintaining ECM hydration [8, 72]. GAGs are hydrophilic structures, assuming an extended conformation, inflating interfibrillar spaces, forming channels where water molecules move and enabling matrices to resist high compressive forces [8, 19, 21].

In the present work, Fourier Transform Infrared Spectroscopy and Raman Spectroscopy techniques were used to investigate the possible contribution of water to the mutability phenomenon. FT-IR data regarding the intensity ratio of amide I/amide II and the height of the absorption band in the 3,100–3,600 cm^{-1} region suggest that water exudation could be involved in the change from the standard to the stiff states, since these tissues have a high content of O–H groups. However, we must keep in mind that the estimated penetration depth (0.15 μm) to which the sample is probed in ATR-FT-IR means that we are at the surface of CDL. Taking advantage of the fact that Raman confocal microscopy allows us to focus on different planes below the sample surface, depth analysis of CDLs was performed. Raman results at different depths are in agreement with FTIR data. The water content of stiff CDLs increases from the surface through the interior, suggesting water exudation. In standard and compliant CDLs the water content in the interior is higher than on the surface.

Attempts to confirm water exudation by using MRI failed due to the small size of the CDLs. Water exudation, is not exclusive to the CDL, since it has been observed in articular cartilage [73–75], in mammalian tendon [76, 77], in intervertebral disc [78], and in other MCT, namely excised holothurian dermis during stiffening [72]. Tamori et al. [72] adduced evidence supporting the view that water exudation resulted from the release of extracellular water molecules that had been previously bound through electrostatic forces, and was caused by changes in non-covalent intermolecular linkages that underpinned tissue stiffening [72]. For example, water molecules bound to GAG side-chains might be displaced by stronger interactions between these chains and putative effector macromolecules such as tensilin, resulting in water exudation.

Our observation that the pattern of water distribution was similar in standard and compliant CDLs suggests that the corresponding tissues are not morphologically different, and are in agreement with our previous ultrastructural findings [5]. As in the investigation by Tamori et al. [72] on holothurian dermis, we found evidence of water exudation under stiffening conditions, but while they measured total water loss we were able to identify the existence of a water concentration gradient. We believe that what we call here "exudated water" may have a rather complex composition, due to the presence of other ECM components released during the stiffening process.

5 Conclusions

This investigation has revealed previously unreported biochemical differences between experimentally induced mechanical states of the sea urchin CDL, which simulate the mutability of the tissue in vivo.

The CDL ECM is a composite structure comprising a dense array of collagen fibrils, PGs, GAGs, water and other glycoproteins. We found that the fibrillar collagen has strong biochemical similarities to mammalian collagen type I, as suggested by FTIR and Raman data. CDL GAGs were found to be sulphated. Although these may be involved in mutability, since they serve as binding sites for molecules responsible for interfibrillar cohesion, they are polyanionic molecules whose electrostatic properties render them osmotically active. When the CDL shifts from the standard to the stiff state, stronger interactions between GAGs and effector proteins (such as tensilin), may expel water molecules.

Our results also demonstrate that CDL mutability does not involve the synthesis of new ECM components, but that adjustments of tissue hydration may occur during shifts in mechanical state.

Although there are similarities between the mutability of the CDL ECM and the human cervix stroma during pregnancy, the time scale is completely different: 1 s to a few minutes in the CDL and hours to days in the cervix. It is highly unlikely that CDL collagen and GAGs are degraded and synthesized in such a short time. As has been inferred with regard to other echinoderm MCTs, the mechanism of CDL mutability seems to depend on molecular rearrangement rather than remodelling.

A broader understanding of CDL mutability could open new perspectives for the development of dynamic and reversible biomaterials enhancing tissue regeneration.

References

1. Motokawa T (1984) Connective tissue catch in echinoderm. Biol Rev 59:255–270
2. Wilkie IC (2005) Mutable collagenous tissue: overview and biotechnological perspective. In: Matranga V (ed) Echinodermata. Progress in molecular and subcellular biology, vol 39. Subseries, marine molecular biotechnology. Springer-Verlag, pp 219–248
3. Barbaglio A, Tricarico S, Ribeiro A, Sugni M, Wilkie IC, Barbosa M, Bonasoro F, Carnevali MDC (2011) The mechanically adaptive connective tissue of echinoderms: their potential for bio-innovation in applied technology and ecology. Mar Environ Res 76(2012):108–113
4. Wilkie IC, Carnevali MDC, Bonasoro F (1992) The compass depressors of *Paracentrotus lividus* (Echinodermata, Echinoida): ultrastructural and mechanical aspects of their variable tensility and contractility. Zoomorphology 112:143–153
5. Ribeiro AR, Barbaglio A, Benedetto CD, Ribeiro CC, Wilkie IC et al (2011) New insights into mutable collagenous tissue: correlations between the microstructure and mechanical state of a sea-urchin ligament. PLoS ONE 6:e24822
6. Shoulder MD, Raines RT (2009) Collagen structure and stability. Annu Rev Biochem 78:929–958
7. Brinckmann J, Notbohm H, Muller PK (2005) Collagen: primer in structure, processing and assembly. Springer, Berlin
8. Frantz C, Stewart K, Weaver VM (2010) The extracellular matrix at a glance. J Cell Sci 123:4195–4200
9. Exposito J-Y, Cluzel C, Garrone R, Lethias C (2002) Evolution of collagens. Anat Rec 268:302–316
10. Trotter JA, Thurmond FA, Koob TJ (1994) Molecular structure and functional morphology of echinoderm collagen fibrils. Cell Tissue Res 275:451–458
11. Kadler KE, Holmes DF, Trotter JA, Chapman JA (1996) Collagen fibril formation. Biochem J 316:1–11
12. D'Alessio M, Ramirez F, Suzuki HR, Solursh M, Gambino R (1990) Cloning of a fibrillar collagen gene expressed in the mesenchymal cells of the developing sea urchin embryo. J Biol Chem 265:7050–7054
13. Cluzel C, Lethias C, Garrone R, Exposito J-Y (2000) Sea urchin fibrillar collagen 2α chain participates in heterotrimeric molecules of $(1\alpha)_2$ 2α stoichiometry. Matrix Biol 19:545–547
14. Cluzel C (2001) Characterization of fibrosurfin, an interfibrillar component of sea urchin catch connective tissues. J Biol Chem 276:18108–18114
15. Trotter JA, Koob TJ (1989) Collagen and proteoglycan in a sea urchin ligament with mutable collagenous properties. Cell Tissue Res 258:527–539
16. Trotter JA, Lyons-Levy G, Thurmond FA, Koob TJ (1995) Covalent composition of collagen fibrils from the dermis of the sea cucumber, *Cucumaria frondosa*, a tissue with mutable mechanical properties. Comp Biochem Physiol 112A:463–478
17. Tipper J, Lyons-Levy G, Atkinson M, Trotter J (2002) Purification, characterization and cloning of tensilin, the collagen-fibril

18. binding and tissue-stiffening factor from *Cucumaria frondosa* dermis. Matrix Biol 21:625–635
18. Koob TJ, Koob-Emunds MM, Trotter JA (1999) Cell-derived stiffening and plasticizing factors in sea cucumber (*Cucumaria Frondosa*) dermis. J Exp Biol 202:2291–2301
19. Junqueira L (1983) Biology of collagen-proteoglycan interaction. Arch Histol Jpn 46:589–629
20. Erlinger R, Welsch U, Scott JE (1993) Ultrastructural and biochemical observations on proteoglycans and collagen in the mutable connective tissue of the feather star *Antedon bifida* (Echinodermata, Crinoidea). J Anat 183:1–11
21. Scott JE (1998) Proteoglycan-fibrillar collagen interactions. J Biochem 252:313–323
22. Kariya Y, Watabe S, Hashimoto K (1990) Occurrence of chondroitin sulphate E in glycosaminoglycan isolated from the body wall of sea cucumber *Stichopus japonicus*. J Biol Chem 265:5081–5085
23. Carnevali MDC, Bonasoro F (2001) Introduction to the biology of regeneration in echinoderms. Microsc Res Tech 55:365–368
24. Carnevali MDC, Bonasoro F (2001) A microscopic overview of crinoid regeneration. Microsc Res Tech 55:403–426
25. Björnsson S (1998) Quantitation of proteoglycans as glycosaminoglycans in biological fluids using an Alcian Blue dot blot analysis. Anal Biochem 256:229–237
26. Garnjanagoonchorn W, Wongekalak L, Engkagul A (2007) Determination of chondroitin sulfate from different sources of cartilage. Chem Eng Process 46(5):465–471
27. Timmons B, Akins M, Mahendroo M (2010) Cervical remodeling during pregnancy and parturition. Trends Endocr Met 21:353–361
28. Winkler M, Rath W (1999) Changes in the cervical extracellular matrix during pregnancy and parturition. J Perinat Med 27:45–60
29. Schlembach D, Mackay L, Shi L, Maner WL, Garfield RE et al (2009) Cervical ripening and insufficiency: from biochemical and molecular studies to in vivo clinical examination. Eur J Obstet Gynecol Reprod Biol 144:S70–S76
30. House M, Kaplan DL, Socrate S (2009) Relationships between mechanical properties and extracellular matrix constituents of the cervical stroma during pregnancy. YSPER 33:300–307
31. Belbachir K, Noreen R, Gouspillou G, Petibois C (2009) Collagen types analysis and differentiation by FTIR spectroscopy. Anal Bioanal Chem 395:829–837
32. Petibois C, Gouspillou G, Wehbe K, Delage J-P, Déléris G (2006) Analysis of type I and IV collagens by FT-IR spectroscopy and imaging for a molecular investigation of skeletal muscle connective tissue. Anal Bioanal Chem 386:1961–1966
33. Franco CF, Santos R, Coelho AV (2011) Exploring the proteome of an echinoderm nervous system: 2-DE of the sea star radial nerve cord and the synaptosomal membranes subproteome. Proteomics 11:1359–1364
34. Santos R, Costa G, Franco C, Gomes-Alves P, Flammang P et al (2009) First Insights into the Biochemistry of Tube Foot Adhesive from the Sea Urchin *Paracentrotus lividus* (Echinoidea, Echinodermata). Mar Biotechnol 11:686–698
35. Larsen M, Cordwell S, Roepstorff P (2002) Graphite powder as an alternative or supplement to reversed-phase material for desalting and concentration of peptide mixtures prior to matrix-assisted laser desorption/ionization-mass spectrometry. Proteomics 2:1277–1287
36. Sea Urchin Genome Sequencing Consortium, Sodergren E, Weinstock GM, Davidson EH, Cameron RA et al (2006) The genome of the sea urchin *Strongylocentrotus purpuratus*. Science 314:941–952
37. Plepis A, Goissis G, DasGupta D (1996) Dielectric and pyroelectric characterization of anionic and native collagen. Polym Eng Sci 36:2932–2938

38. Goissis G, Piccirili L, Goes JC, de Guzzi Plepis AM, Das-Gupta DK (1998) Anionic collagen: polymer composites with improved dielectric and rheological properties. Artif Organs 22:203–209

39. Jastrzebska M, Wrzalik R, Kocot A, Zalewska-Rejdak J, Cwalina B (2003) Raman spectroscopic study of glutaraldehyde-stabilized collagen and pericardium tissue. J Biomater Sci Polym Ed 14:185–197

40. Osada M, Gniadecka M, Wulf HC (2004) Near-infrared Fourier transform Raman spectroscopic analysis of proteins, water and lipids in intact normal stratum corneum and psoriasis scales. Exp Dermatol 13:391–395

41. Haston JL (2003) Raman microscopy and X-ray diffraction, a combined study of fibrillin-rich microfibrillar elasticity. J Biol Chem 278:41189–41197

42. Tuma R (2005) Raman spectroscopy of proteins: from peptides to large assemblies. J Raman Spectrosc 36:307–319

43. Cheng W-T, Liu M-T, Liu H-N, Lin S-Y (2005) Micro-Raman spectroscopy used to identify and grade human skin pilomatrix-oma. Microsc Res Tech 68:75–79

44. Movasaghi Z, Rehman S, Rehman IU (2007) Raman spectros-copy of biological tissues. Appl Spectroscopy Revs 42:493–541

45. Jackson M, Choo LP, Watson PH, Halliday WC, Mantsch HH (1995) Beware of connective tissue proteins: assignment and implications of collagen absorptions in infrared spectra of human tissues. Biochim Biophys Acta 1270:1–6

46. Bryan MA, Brauner JW, Anderle G, Flach CR, Brodsky B et al (2007) FTIR studies of collagen model peptides: complementary experimental and simulation approaches to conformation and unfolding. J Am Chem Soc 129:7877–7884

47. Barth A (2007) Infrared spectroscopy of proteins. Biochimica et Biophysica Acta (BBA) Bioenergetics 1767:1073–1101

48. Wehbe K, Pinneau R, Moenner M, Déléris G, Petibois C (2008) FT-IR spectral imaging of blood vessels reveals protein second-ary structure deviations induced by tumor growth. Anal Bioanal Chem 392:129–135

49. Noreen R, Chien C–C, Delugin M, Yao S, Pineau R et al (2011) Detection of collagens in brain tumors based on FTIR imaging and chemometrics. Anal Bioanal Chem 401:845–852

50. Byler M, Susi H (1986) Examination of the secondary structure of proteins by deconvolved FTIR spectra. Biopolym 25:469–487

51. Kong J, Yu S (2007) Fourier transform infrared spectroscopic analysis of protein secondary structures. Acta Bioc et Biophys Sinica 39(8):549–559

52. Jackson M, Mantsch HH (1995) The use and misuse of FTIR spectroscopy in the determination of protein structure. Crit Rev Bioch Mol Biol 30(2):95–120

53. Canty E, Kadler K (2002) Collagen fibril biosynthesis in tendon: a review and recent insights. Comp Biochem Physiol A 133:979–985

54. Camacho NP, West P, Torzilli PA, Menndelsohn R (2001) FTIR microscopic imaging of collagen and proteoglycan in bovine cartilage. Biopolym 62:1–8

55. Potter K, Kidder LH, Levin IW, Lewis EN, Spencer RG (2001) Imaging of collagen and proteoglycan in cartilage sections using Fou-rier transform infrared spectral imaging. Arthritis Rheum 44:846–855

56. Chen S, Xue C, Yin L, Tang Q, Yu G (2010) Comparison of struc-tures and anticoagulant activities of fucosylated chondroitin sul-phates from different sea cucumbers. Carbohyd Polym 83:688–696

57. Ellis R, Green E, Winlove CP (2009) Structural analysis of gly-cosaminoglycans and proteoglycans by means of Raman micro-spectrometry. Connect Tissue Res 50:29–36

58. Ishwar AR, Jeong KJ, Panitch A, Akkus O (2009) Raman spec-troscopic investigation of peptide-glycosaminoglycan interac-tions. Appl Spectrosc 63:636–641

59. Cinelli LP, Vilela-Silva A-CES, Mourão PAS (2009) Seminal fluid from sea urchin (Lytechinus variegatus) contains complex sulphated polysaccharides linked to protein. Comp Biochem Physiol 154:108–112

60. Mainreck N, Brézillon S, Sockalingum GD, Maquart F-X, Manfait M et al (2010) Rapid characterization of glycosamino-glycans using a combined approach by infrared and Raman mi-crospectroscopies. J Pharm Sci 100:441–450

61. Yamada S, Sugahara K, Ozbek S (2011) Evolution of glycos-aminoglycans: comparative biochemical study. Commun Integr Biol 4:150–158

62. Medeiros GF, Mendes A, Castro RA, Baú EC, Nader HB et al (2000) Distribution of sulphated glycosaminoglycans in the ani-mal kingdom: widespread occurrence of heparin-like compounds in invertebrates. Biochim Biophys Acta 1475:287–294

63. Maul H, Mackay L, Garfield RE (2006) Cervical ripening: bio-chemical, molecular, and clinical considerations. Clin Obstet Gynecol 49:551–563

64. Myers K, Socrate S, Tzeranis D, House M (2009) Changes in the biochemical constituents and morphologic appearance of the human cervical stroma during pregnancy. Eur J Obstet Gynecol Reprod Biol 144:82–89

65. Read CP, Word RA, Ruscheinsky MA, Timmons BC, Mahendroo MS (2007) Cervical remodeling during pregnancy and parturi-tion: molecular characterization of the softening phase in mice. Reprod 134:327–340

66. Akins ML, Luby-Phelps K, Bank RA, Mahendroo M (2011) Cervical softening during pregnancy: regulated changes in col-lagen cross-linking and composition of matricellular proteins in the mouse. Biol Reprod 84:1053–1062

67. Sulea D, Micutz M, Albu MG, Staicu T, Leca M (2011) Colla-gen-thuja tincture biomaterials for wound treatment. 2. Hydrogels and porous matrices. Rev Roum Chim 56:129–136

68. Singh P, Benjakul S, Maqsood S, Kishimura H (2011) Isolation and characterisation of collagen extracted from the skin of striped catfish (Pangasianodon hypophthalmus). Food Chem 124:97–105

69. Kittiphattanabawon P, Benjakul S, Visessanguan W, Shahidi F (2010) Isolation and characterization of collagen from the carti-lages of brownbanded bamboo shark (Chiloscyllium punctatum) and blacktip shark (Carcharhinus limbatus). Lwt-Food Sci Technol 43:792–800

70. Brooks J (2002) The major yolk protein in sea urchins is a transferrin-like. Iron Binding Protein Dev Biol 245:1–12

71. Noll H, Alcedo J, Daube M, Frei E, Schiltz E, Hunt J, Humphries T, Matranga V et al (2007) The toposome, essential for sea urchin cell adhesion and development, is a modified iron-less calcium-binding transferrin. Dev Biol 310:54–70

72. Tamori M, Takemae C, Motokawa T (2010) Evidence that water exudes when holothurian connective tissue stiffens. J Exp Biol 213:1960–1966

73. Shapiro E (2001) Water distribution patterns inside bovine articular cartilage as visualized by 1H magnetic resonance imaging. Osteoarthr Cartil 9:533–538

74. Berberat JE, Nissi MJ, Jurvelin JS, Nieminen MT (2009) Assessment of interstitial water content of articular cartilage with T1 relaxation. Magn Reson Imaging 27:727–732

75. Liess C (2002) Detection of changes in cartilage water content using MRI T2-mapping in vivo. Osteoarthr Cartil 10:907–913

76. James R, Kesturu G, Balian G, Chhabra AB (2008) Tendon: biology, biomechanics, repair, growth factors, and evolving treatment options. J Hand Surg 33:102–112

77. Wellen J (2004) Application of porous-media theory to the investigation of water ADC changes in rabbit Achilles tendon caused by tensile loading. J Magn Reson 170:49–55

78. Matsumura Y, Kasai Y, Obata H, Matsushima S, Inaba T et al (2009) Changes in water content of intervertebral discs and paravertebral muscles before and after bed rest. J Orthop Sci 14:45–50